A Precise Orbit Determination Technique to Refine Spacecraft Mechanical Modeling

Journal:	*Journal of Spacecraft and Rockets*
Manuscript ID	2020-08-A34922.R1
Manuscript Type:	Full Paper
Date Submitted by the Author:	n/a
Complete List of Authors:	Cascioli, Gael; Sapienza University of Rome, Department of Mechanical and Aerospace Engineering Genova, Antonio; Sapienza University of Rome, Department of Mechanical and Aerospace Engineering
Subject Index Category:	33200 Spacecraft Dynamics < 30000 GUIDANCE, CONTROL, AND DYNAMICS TECHNOLOGY, 32500 Navigation < 30000 GUIDANCE, CONTROL, AND DYNAMICS TECHNOLOGY, 70700 Space Experiments < 70000 SPACE TECHNOLOGY

A Precise Orbit Determination Technique to Refine Spacecraft Mechanical Modeling

Gael Cascioli * and Antonio Genova.†
Sapienza University of Rome, Via Eudossiana 18, 00184 Rome, Italy

The precise orbit determination of interplanetary spacecraft requires an accurate modeling of the center of mass position with respect to the antenna phase center. Unpredicted variations of this relative position due to events that redistribute the spacecraft mass affect significantly the precision of the radio tracking measurements by inducing spurious Doppler signals. We present a technique to calibrate uncompensated Doppler signals caused by time-varying offsets between the spacecraft center of mass and antenna phase center. This method is applied to the precise orbit determination of the Mars Reconnaissance Orbiter to correct Doppler signatures induced by high-frequency movements of the center of mass due to the re-orientation of the gimbaled appendages (i.e., solar arrays and high gain antenna).

Nomenclature

c	=	speed of light, ms^{-1}
df	=	frequency shift, Hz
f	=	frequency, Hz
G	=	observation model
H	=	mapping matrix
$\tilde{H}_i$	=	mapping matrix i-th row
$\hat{\mathbf{I}}$	=	line-of-sight unit vector
M	=	mass, kg
q	=	generic parameter
R^i	=	i-th element rotation matrix
R	=	observation noise covariance matrix
$\mathbf{r}$	=	position vector
X	=	state vector
x	=	state deviation vector

*PhD Student, Department of Mechanical and Aerospace Engineering , Via Eudossiana 18, 00184 Rome, Italy.
†Assistant Professor, Department of Mechanical and Aerospace Engineering , Via Eudossiana 18, 00184 Rome, Italy.

y = residuals vector

ρ = line-of-sight distance, m

Φ = state transition matrix

ω = angular velocity vector

Subscripts

APP = appendage

BP = baseplate

COM = center of mass

HGA = high gain antenna

IG = inner gimbal

OG = outer gimbal

PC = phase center

SAMX = solar array -x direction

SAPX = solar array +x direction

SBF = spacecraft body fixed reference frame

I. Introduction

Accurate calibrations of measurement and model error sources are fundamental for the precise orbit determination (POD) of interplanetary spacecraft. The accurate modeling of the relative position of the phase center of the antenna (typically high gain antenna, HGA) and the spacecraft center of mass (CoM) plays a key role. The trajectory of the spacecraft CoM is integrated in the dynamical equations, and the radiometric observables (*e.g.*, Doppler data) rely on the location of the antenna phase center. Mismodeling in the static and time-varying evolution of the relative distance between the spacecraft CoM and antenna phase center induces significant unpredicted Doppler shifts that lead to large errors in the spacecraft reconstructed trajectory. A very efficient technique to fully compensate these effects is based on the support of dedicated accelerometers onboard the spacecraft. The ESA mission Jupiter icy moons explorer (JUICE), for example, will host aboard an accelerometer to retrieve the Doppler signal caused by the propellant sloshing in the spacecraft tank. The architecture of this instrument is based on the Italian Spring Accelerometer (ISA) onboard the Mercury Planetary Orbiter (MPO) of the joint ESA/JAXA mission BepiColombo that was designed to measure the accelerations due to non-conservative forces acting on the spacecraft dynamics across the harsh Mercury's environment [1, 2]. By knowing precisely the location of an arbitrary reference point of the antenna with respect to the accelerometer vertex in the spacecraft reference frame (*i.e.*, Schulte vector [3]), and by measuring the effect of the non-gravitational forces through the accelerometers, the entire orbit determination process can be referred to the accelerometer reference

point, instead of the CoM. This approach is fully independent of the knowledge of the relative distance between the antenna phase center and the spacecraft CoM.

Interplanetary spacecraft, however, are not commonly equipped with sophisticated onboard accelerometers. Therefore, different techniques have been proposed to precisely determine the location of the CoM in the spacecraft reference frame. Two independent classes can be distinguished: active techniques that require planned spacecraft attitude maneuvers that yield the observability of the perturbations induced by CoM position mismodeling [4, 5]; and passive techniques that are based on the processing of optical observations of the spacecraft orientation [6, 7], accelerometer readings [8] gyroscopes readings [9] and radio tracking data [10, 11]. These calibration techniques are not well-suited for spacecraft that include gimbaled appendages, since the re-configuration of the movable panels provide unpredicted variations of the CoM position. Accurate radio tracking data are highly sensitive to the mismodeling of the relative distance between the CoM and phase center antenna. Cutting-edge radio tracking systems have been designed to obtain Doppler data accuracy up to 30 $\mu m\ s^{-1}$ @10-s integration time (e.g., [2]), and a precise compensation of the CoM displacement-induced perturbations is then fundamental. A full calibration of these effects would require a perfect knowledge of the spacecraft mechanical model. However, uncertainties related to the spacecraft mass distribution or to each component location affect significantly these *a priori* assumptions. We present a calibration technique that allows refining the spacecraft mechanical model through the processing of the radio tracking Doppler data. By using this approach to the reanalysis of the Mars Reconnaissance Orbiter (MRO) tracking data, we obtain an updated spacecraft modeling that is crucial for the precise orbit determination of the radio science investigation.

The work is structured as follows: in Sec. II we describe the Doppler perturbation induced by the CoM time-variable position, in Sec. III we detail the proposed calibration method, in Sec. IV we describe the MRO mission and spacecraft mechanical model, and in Sec. V we present and discuss the results of the application of the proposed calibration method to nearly 2 years of MRO Doppler data.

II. Modeling of the Doppler signal due to time-varying CoM location

The scientific return of space robotic missions strongly relies on the accuracy of the spacecraft orbit reconstruction. A precise knowledge of the probe's trajectory is required by several scientific investigations including altimetry and imaging to georeference their datasets. The precise orbit determination (POD) is accomplished through the processing of radio tracking data that allows adjusting the dynamical force models. The *a priori* dynamical model is used to retrieve a first-guess trajectory and the associated predicted measurements (*computed observables*). By minimizing the discrepancies (*residuals*) between *computed observables* and *observed observables* (*i.e.* the actual measurements collected at the ground station), the POD algorithm based on a least-squares filter enables the estimation of the parameters of interest that affect the spacecraft dynamics.

Deep space tracking for interplanetary navigation is obtained through the transmission of a X- ($\sim 7.2 GHz$) or

Ka-band ($\sim 34GHz$) radio signal from an Earth's station to the probe, which receives and sends it coherently back in X- ($\sim 8.4GHz$) or Ka-band ($\sim 32GHz$). The Doppler observable is acquired at the Earth's station by measuring the frequency change between the transmitted and received signal. The formulation for the instantaneous* Doppler frequency shift df as a function of the carrier frequency f and the radio beam propagation velocity (equal to the speed of light c in vacuum) is:

$$\frac{df}{f} = \frac{1}{c}\frac{d\rho}{dt} \tag{1}$$

where $d\rho/dt$ is the relative velocity along the spacecraft-Earth's station line-of-sight. This relative velocity is, more precisely, referred to the phase center of the spacecraft antenna, which is the reference point of the actual observations. Since the POD process is based on the integration of the spacecraft CoM trajectory, the *computed* observables must accurately account for the relative position of the phase center with respect to the spacecraft CoM. Mismodeling of the time-varying distance between the spacecraft CoM and antenna phase center may cause significant artifacts and signatures in the Doppler data residuals. The line-of-sight position of the HGA phase center, ρ_{PC} can be expressed as follows:

$$\rho_{PC} = [\mathbf{r}_{COM} + (\mathbf{r}_{PC} - \mathbf{r}_{COM})] \cdot \hat{\mathbf{l}} = \left[\mathbf{r}_{COM} + \mathbf{r}_{PC_{rel}}\right] \cdot \hat{\mathbf{l}} \tag{2}$$

where $\mathbf{r}_{COM}$ and $\mathbf{r}_{PC}$ are the inertial position vectors of the CoM and phase center, respectively, $\mathbf{r}_{PC_{rel}}$ is the position of the phase center relative to the CoM and $\hat{\mathbf{l}}$ is the Earth-spacecraft line-of-sight unit vector. Thus, by assuming as a first approximation a time invariant $\hat{\mathbf{l}}$, the relative velocity is given by:

$$\frac{d(\rho_{PC})}{dt} = \left[\dot{\mathbf{r}}_{COM} + \dot{\mathbf{r}}_{PC_{rel}} + \boldsymbol{\omega} \times \mathbf{r}_{PC_{rel}}\right] \cdot \hat{\mathbf{l}} \tag{3}$$

where $\boldsymbol{\omega}$ is the inertial angular velocity of $\mathbf{r}_{PC_{rel}}$. An accurate knowledge of the HGA phase center location is then fundamental to computing the Doppler observable, which relies on the temporal evolution of the spacecraft attitude ($\boldsymbol{\omega} \times \mathbf{r}_{PC_{rel}}$) and of its relative position with respect to the spacecraft CoM ($\dot{\mathbf{r}}_{PC_{rel}}$). The former effect has been extensively investigated in previous studies (e.g., [10]) since it may cause strong signals because of the large spacecraft angular velocities. The contribution of the time-varying CoM-phase center location, on the other hand, has been poorly studied but it is also detectable with the increased accuracy of the latest radiometric tracking systems. Variations of the relative distance between the antenna phase center and the spacecraft CoM are induced by a geometrical change of the antenna orientation through gimbals and by movable appendages, including solar arrays and HGA, that lead to a spacecraft mass redistribution.

Figure 1 shows the Doppler shift of the MRO radio tracking data caused by fully neglecting the phase center-CoM distance (dashed line) and its temporal evolution (solid line). The Doppler signal due to an error in the antenna phase

*Note that the actual Doppler observable consists in the measurement of the integral mean of the frequency shift over a specific count time [12]. We adopt the time continuous mathematical formulation for the sake of notation simplicity.

center location with respect to the spacecraft CoM is amplified by the attitude angular velocities. Therefore, an accurate knowledge of this distance is required to correctly fit the Doppler data. Furthermore, the reorientation of movable appendages leads to high-frequency variations of this distance that are detectable in the case of the MRO radio tracking data. We present here a technique to compensate both effects in the POD analysis, enhancing the orbit reconstruction of spacecraft.

III. Methods

An accurate knowledge of the spacecraft CoM location in the spacecraft reference frame is achieved by accounting for the CoM position of each element of the engineering model including the bus, solar panels, and HGA. The location of the spacecraft CoM is updated, for example, after orbital or reaction wheel desaturation maneuvers that affect the mass distribution within the bus. Mismodeling of the CoM location of the spacecraft elements may result in unpredicted signals in the Doppler data. By opportunely implementing the kinematic chain of the antenna phase center in our POD analysis, we include the estimation of the CoM position vectors of each element to fully compensate these possible perturbations.

The determination of these parameters of interest is accomplished through the POD process that enables the adjustment of a state vector, X, which is a set of parameters related to the dynamical or observation modeling. In the linearized POD problem, the state *deviation* vector x_0 is the difference between the actual and reference state at a specific reference epoch, and it is related to the residuals y_i at time t_i as follows [13, 14]:

$$y_i = \tilde{H}_i \Phi(t_i, t_0) x_0 + \epsilon_i \tag{4}$$

where Φ is the state transition matrix, ϵ_i is the observation noise at time t_i, and $\tilde{H}$ is the matrix of partial derivatives of the observation model $G(t)$ with respect to the state vector $\left(\tilde{H}_i = \frac{\partial G(t_i)}{\partial X_i}\right)$.

By grouping Eq. 4 for all observation times, and by introducing the mapping matrix H, whose rows consist of the terms $\tilde{H}_i \Phi(t_i, t_0)$, we can rewrite the observation equation

$$y = H x_0 + \epsilon. \tag{5}$$

The weighted least-squares solution of Eq. 5, and thus the estimate of the state deviation vector $\hat{x}_0$ is given by:

$$\hat{x}_0 = \left(H^T R^{-1} H\right)^{-1} H^T R^{-1} y \tag{6}$$

where R is the covariance matrix of the observation noise. The adjusted state vector in our analysis includes the parameters related to the kinematic model of the spacecraft. A thorough implementation of the partial derivatives of the

Doppler measurement with respect to the location of each element CoM, q, through Eqs. 1 and 3 leads to the following:

$$\frac{\partial G}{\partial q} = \frac{f}{c}\frac{d}{dt}\left[\frac{\partial \mathbf{r}_{PC_{rel}}}{\partial q}\cdot\hat{\mathbf{l}}\right]. \tag{7}$$

The Doppler signal due to time-varying CoM location is opportunely calibrated by estimating these additional parameters in the POD process. This formulation is based on the assumption that the rotations of the movable panels do not affect significantly the spacecraft trajectory, and thus $\partial \mathbf{r}_{CoM}/\partial q = 0$.

IV. CoM Modeling of the MRO spacecraft

The MRO spacecraft has been orbiting Mars since March 2006 and, at the date of this work, is still operative. The main goal of the mission is a comprehensive investigation of the planet Mars through the suite of instruments hosted onboard [15]. The analysis of the radio tracking data acquired by the Earth's stations enabled the determination of Mars' static and time-varying gravity field [16–19].

MRO is in an eccentric sun-synchronous orbit about Mars with the apoapsis altitude of 320 km, the periapsis altitude of 255 km, and the ascending node local solar time at 3PM. The spacecraft structure is 981 kg and the propellant mass at launch was $\sim$ 1199 kg. Figure 2 shows the spacecraft modeling adopted in this study that is based on the frame kernels archived on the JPL's Navigation and Ancillary Information Facility (NAIF) [†]. Our model consists of: (**1**) the spacecraft bus; (**2**) two 10-m^2 solar panels (solar array +x, SAPX , and solar array -x, SAMX); (**3**) a 3-m HGA; and (**4**) the fuel and helium tank [20]. The HGA is steerable with inner and outer gimbals to enable precise pointing to Earth, and the solar panels are also movable to produce sufficient power onboard.

This spacecraft design was conceived to accomplish the challenging mission objectives that require an highly accurate knowledge of the spacecraft attitude. Precise pointing of the instrumentation deck to observe specific targets on the Martian surface with the onboard camera and radar, and the orientation of the HGA to the Earth and the solar panels to the Sun result in a tight and demanding scheduling of attitude operations. The reorientation of the instrumentation deck yields off-nadir angles up to ± 30°, and continuous yaw adjustments to compensate the relative motion of the planetary surface underneath the spacecraft. The solar panels are rotated independently through dedicated gimbals attached directly to the spacecraft structure to guarantee the input solar power along the MRO mid-afternoon sun-synchronous orbit. The transmission of the scientific data to the ground requires a second independent attitude of the HGA that relies on the relative direction of the Earth with respect to the orbital plane [20, 21].

Solar panels and HGA rotations are responsible for a mass redistribution of the spacecraft system that causes a

[†]available at `https://naif.jpl.nasa.gov/pub/naif/MRO/kernels/fk/mro_v15.tf`

significant offset of its CoM location. By using the mechanical model described in the following section, we recovered the amount of this displacement that reaches up to 15 cm over relatively short time spans (~10 minutes, as depicted in Fig. 4).

A. Spacecraft Mechanical Model

A detailed mechanical model of the spacecraft is fundamental to computing the instantaneous CoM position. In this section, we adopt a spacecraft model based on the work by Genova *et al.* [18]. The CoM position in the spacecraft body fixed reference frame (SBF) is:

$$\mathbf{r}_{CoM}^{SBF} \sum_i M_i = \sum_i M_i \mathbf{r}_i^{SBF} \tag{8}$$

where $\mathbf{r}_i^{SBF}$ and M_i are the position (in SBF) and mass of each spacecraft element, respectively. In our model we exclusevly account for the two solar arrays, HGA, fuel tank, helium tank and spacecraft bus since other elements do not contribute significantly to the computation of the CoM location. Solar arrays and HGA are movable panels, therefore, their kinematics can be defined as follows

$$\mathbf{r}_{APP}^{SBF} = \mathbf{r}_1 + R^2\mathbf{r}_2 + \cdots + R^n\mathbf{r}_n. \tag{9}$$

Here the position of each appendage, $\mathbf{r}_{APP}^{SBF}$, is obtained through a series of n rotations and translations of the sub-elements that form its kinematic chain. The position vector of each sub-element i, $\mathbf{r}_i$, is expressed in its own reference frame that has a certain orientation with respect to the SBF. The first sub-element 1 is expressed, for example, directly in SBF and its rotation matrix is an identity matrix. A generic rotation matrix R^i from the i reference frame to SBF allows transforming a vector from the i reference frame ($\mathbf{r}$) to the SBF through $\mathbf{r}^{SBF} = R^i\mathbf{r}$.

An accurate implementation of the kinematics chain that accounts for the gimbaled appendages is presented in the MRO reference frame kernels[‡]. Figure 3 shows the concatenated reference frames that are either fixed or time-varying (indicated in Fig. 3 with solid and dashed lines, respectively). The rotation matrices of the gimbals vary over time accordingly to the measured quaternions of those independent sub-elements[§].

An important difference between the solar arrays and the HGA is the origin of the gimbals, which is located at the origin of the baseplate for the solar arrays but not for the HGA. Therefore, the position vector of each movable panel in the SBF is given by:

[‡]available at `https://naif.jpl.nasa.gov/pub/naif/MRO/kernels/fk/mro_v15.tf`
[§]available at `https://naif.jpl.nasa.gov/pub/naif/MRO/kernels/ck/`

$$\begin{aligned}
\mathbf{r}^{SBF}_{SAPX} &= \mathbf{r}^{SBF}_{SAPX_{BP}} + R^{SAPX}\mathbf{r}_{SAPX} \\
\mathbf{r}^{SBF}_{SAMX} &= \mathbf{r}^{SBF}_{SAMX_{BP}} + R^{SAMX}\mathbf{r}_{SAMX} \\
\mathbf{r}^{SBF}_{HGA} &= \mathbf{r}^{SBF}_{HGA_{BP}} + R^{IG}\mathbf{r}_{IG} + R^{OG}\mathbf{r}_{OG} + R^{HGA}\mathbf{r}_{HGA}
\end{aligned} \tag{10}$$

Here the subscripts BP, IG, and OG stand for baseplate, inner gimbal and outer gimbal, respectively. The position of the fixed mass elements is obtained through a direct translation in the SBF. We will refer to the position of the spacecraft bus, propellant tank and helium tank as $\mathbf{r}_{BUS}$, $\mathbf{r}_{FUEL}$ and $\mathbf{r}_{HELIUM}$, respectively.

By using Eq. 8 in combination with the *a priori* knowledge of the masses and relative positions of each element, and the quaternions for the time-varying rotation matrices, we compute $\mathbf{r}(t)^{SBF}_{CoM}$ at each time required in the POD process. Figure 4 shows the evolution of the CoM position in the SBF $\left\|\mathbf{r}(t)^{SBF}_{CoM}\right\|$, labeled as *CoM*, and the relative position of the HGA with respect to the spacecraft CoM in the SBF $\left\|\mathbf{r}(t)^{SBF}_{HGA} - \mathbf{r}(t)^{SBF}_{COM}\right\|$, labeled as *HGA*, over the time span of a generic MRO orbit. The spacecraft CoM moves with an amplitude of several centimeters over a reduced time span. Furthermore, more interestingly, the relative distance between the CoM and the HGA decreases during Earth's occultation because of the HGA rewind, and increases during tracking visibility to maintain Earth's pointing. This trend shows a significant once-per-orbit periodic pattern that, (as shown in Sec. II) if not properly compensated, induces spurious Doppler signals in the radiometric tracking data.

B. Effect of model uncertainties on MRO Doppler residuals

An accurate correction of the Doppler measurement for the MRO mission is then computed by implementing the model described in Sec. IV. Figure 5 reports the comparison between the MRO Doppler residuals obtained with and without the calibration of the CoM movement. The correction of the observable by using an *a priori* mechanical model of the spacecraft allows mitigating the Doppler shift induced by time-varying CoM location, as shown by Genova *et al.* [18]. An important aspect that this method does not include is the uncertainty associated to the *a priori* information. The knowledge of the spacecraft model is affected by unpredicted errors that may lead to an incorrect mass distribution modeling. The right panel of Figure 5 shows uncompensated MRO Doppler signatures due to the assumed mechanical model of the spacecraft. Similar patterns stand out during several MRO tracking passages that are characterized by high-frequency attitude variations of the whole spacecraft and the movable panels.

The aim of this work is to overcome these limitations by estimating directly an updated and refined mechanical model through the analysis of the Doppler observables to suppress artifacts and perturbations induced by the CoM motion.

V. Refinement of the MRO spacecraft modeling through the radio tracking data processing

The estimation of the locations of each spacecraft element is obtained through the processing of the MRO radio tracking data within a certain time span (*arc*). The POD solution requires an in depth modeling of the dynamical forces acting on the spacecraft trajectory including: (**1**) Mars' gravity field both static (in spherical harmonics to degree and order 120) and time-varying (in spherical harmonics to degree 5); (**2**) tidal interactions of Mars with its satellites and the Sun; (**3**) atmospheric drag; (**4**) solar radiation pressure; (**5**) visible and infrared emission of Mars; and (**6**) gravitational attraction of all the main solar system bodies and Mars' satellites Phobos and Deimos [18].

A. Filter Setup

The MRO radio tracking data were processed in the POD filter with a multi-arc approach [22]. A certain level of inaccuracies in the dynamical model leads to uncompensated signatures in observations that cover a long time span. Orbital maneuvers, for example, strongly affect the dynamical coherency of the trajectory preventing a continuous propagation of the spacecraft orbit. For this reason, the mission time span is divided into adjacent temporal arcs that allows adjusting multiple *states*. In the multi-arc approach the estimated parameters of the entire state are *local* or *global* if they affect a single arc only, or all the arcs, respectively. MRO orbital arcs are 2-3 days long to exclude the periodic orbit correction maneuvers [18].

In this study the geometrical position of each component of the spacecraft mechanical model is estimated as a global parameter with the exception of the CoM position of the fuel, which is treated as a local parameter. This approach allows then accounting for an arc-by-arc variability induced by the fuel consumption after each orbital correction maneuver. A full list of the model parameters retrieved in our POD solution is reported in Table 1. The geometrical positions $\mathbf{r}_{HGA_{BP}}$, $\mathbf{r}_{HELIUM}$, $\mathbf{r}_{SAMX_{BP}}$ and $\mathbf{r}_{SAPX_{BP}}$ are not adjusted in the POD filter because of the lack of Doppler data sensitivity to these parameters. However, we modeled those as *consider* parameters, which are not corrected but their uncertainties and correlations are taken into account into the overall covariance matrix of the POD filter.

B. Results

We present here the updated spacecraft mechanical model obtained by processing a full Martian year of MRO Doppler data. This time interval is representative for all MRO operation conditions during the science mission phase. The analyzed dataset accounts for 341 contiguous arcs from 12 May 2011 to 9 April 2013. The results of our POD solution is reported in Table 2 in terms of corrections with respect to the *a priori* model (*Delta*) and of estimated formal uncertainty of the mechanical model global parameters. The main correction is applied to the solar arrays x component, which is the coordinate aligned with the panel horizontal axis. All the other corrections are of the centimeter level or below with the exception of the y component of $\mathbf{r}_{HGA}$.

Figure 6 reports our arc-by-arc estimates of the fuel tank CoM position along the fuel filling direction (y component

in the SBF) with $3-\sigma$ formal uncertainty. This estimated parameter is well determined over the first half of the dataset, but it is more scattered from June 2012. This result is consistent with the attitude commanded to the MRO spacecraft during the Martian dust storm period [23], when the solar arrays are maintained fixed to reduce atmospheric drag induced perturbations [24]. This attitude configuration yields a significant decrease of the associated Doppler signal, thus strongly degrading the data sensitivity to those effects.

Figure 7 shows the Doppler residuals that are computed by using the estimated spacecraft model. The refined location of the spacecraft elements proves to be extremely effective in suppressing the CoM motion-induced signatures. The Doppler residuals reported in the two top panels correspond to the same dataset of Figure 5. The refined mechanical model estimated directly from the Doppler data efficiently suppresses the residual signatures due to errors in the *a priori* spacecraft modeling. Similar improvements are obtained for all the other analyzed data arcs. The bottom panels of Figure 7 show the magnitude of CoM displacement computed with the refined model and its formal uncertainty (shaded area) over the same orbit covered by the reported Doppler data.

Another important aspect to assess is whether the adjusted mechanical model allows enhancing the estimate of the spacecraft state vector. To compare the overall discrepancies between the spacecraft states (position and velocity) obtained by using the *a priori* and the updated spacecraft model, we report in Figure 8 their Mahalanobis[¶] distance for each arc. The histogram shows the percentage of arcs with estimate differences of the state vector within 4.48 Mahalanobis distance (equivalent to $3-\sigma$ formal uncertainties or 99.73% confidence level of univariate normal distribution). A significant amount of arcs (35.7%) show a larger distance, providing an evidence that the spacecraft orbit is significantly modified by the estimation of the spacecraft modeling. A significant improvement of the Doppler residuals of those arcs suggests, therefore, an enhanced determination of the spacecraft trajectory through the described POD technique.

VI. Conclusions

Cutting-edge tracking technologies will lead to unprecedented levels of accuracy for the reconstruction of spacecraft orbits, by reducing the noise floor of the radiometric link. However, these improvements will provide more stringent requirements on the engineering modeling of the dynamical effects that will be detectable and potentially detrimental to the POD processing.

In this work we proposed a technique to compensate errors in the spacecraft mechanical modeling by adjusting the CoM location, which is especially uncertain for spacecraft with movable appendages. An inaccurate knowledge of the CoM motion causes spurious signals in the Doppler navigation data. After a theoretical analysis of the problem, we developed and applied a CoM estimation strategy, based on the inclusion of the spacecraft kinematics chain in

[¶]The Mahalanobis distance, M, quantifies the distance of a point from a multivariate normal distribution [25]. In the case of a univariate normal distribution this coincides with the euclidean distance scaled with the standard deviation, *i.e.* $1M = 1\sigma, 2M = 2\sigma, \ldots$

the POD solution. The analysis of nearly 2 years of MRO tracking data shows the benefits of our technique, which allows calibrating the uncompensated Doppler signals. The proposed method enables an accurate refinement of the spacecraft mechanical model with an accurate determination of the location of each spacecraft panel including movable appendages.

The updated spacecraft mechanical model has also an impact on the reconstruction of the spacecraft trajectory. The enhancements in the Doppler residuals and the discrepancies in the orbital solution with respect to the case with the *a priori* spacecraft model suggest that the adjusted CoM location enables improved orbital solutions. A better characterization of these improvements, however, is possible with an independent analysis of other scientific data (*altimetry*) that rely on the reconstructed orbits. Our resulting spacecraft model will be used to the analysis of the MRO radio tracking data in a global analysis devoted to enhance our knowledge of Mars' static and time-varying gravity field.

Acknowledgments

This work has been funded by grants of the Italian Ministry of Education, University and Research (MIUR). A.G. thanks S. Goossens (UMBC, CRESST), and E. Mazarico (NASA, GSFC) for their support in the analysis of MRO radio tracking data. G.C. is grateful to D. Durante (Sapienza Università di Roma) for the many fruitful discussions and continuous support and to M. Zannoni (Università di Bologna).

FIGURES AND TABLES

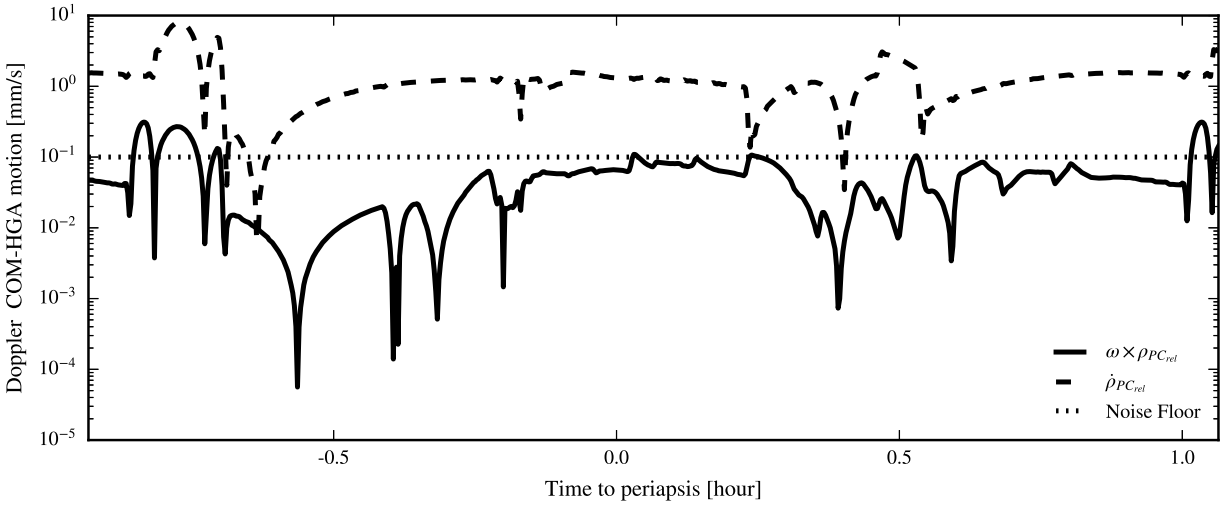

Fig. 1 Doppler effect associated to the CoM displacement

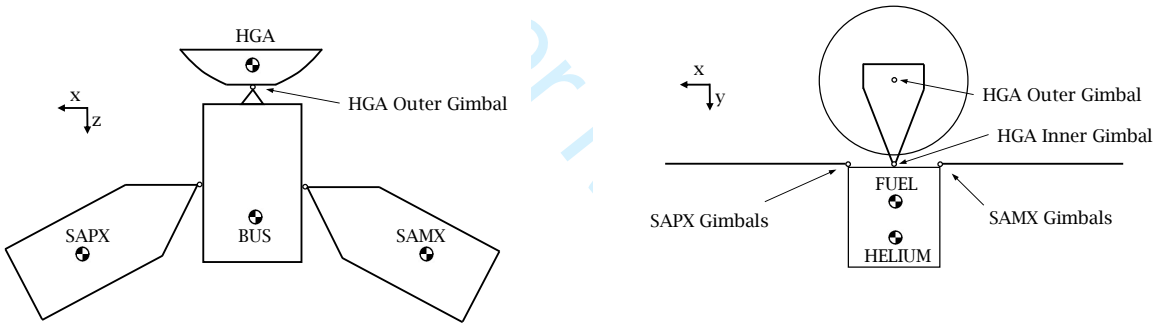

(a) X-Y view **(b) X-Z view**

Fig. 2 MRO Schematic Structure

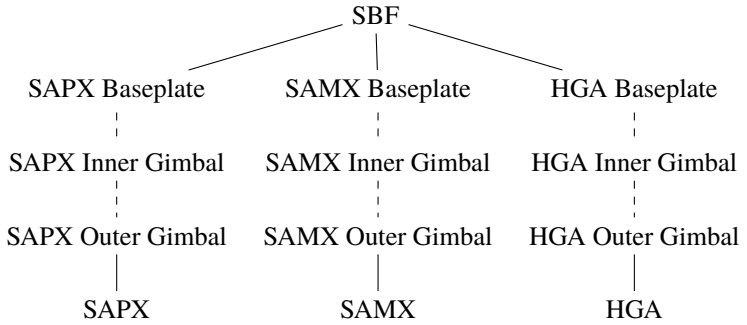

Fig. 3 Reference frames

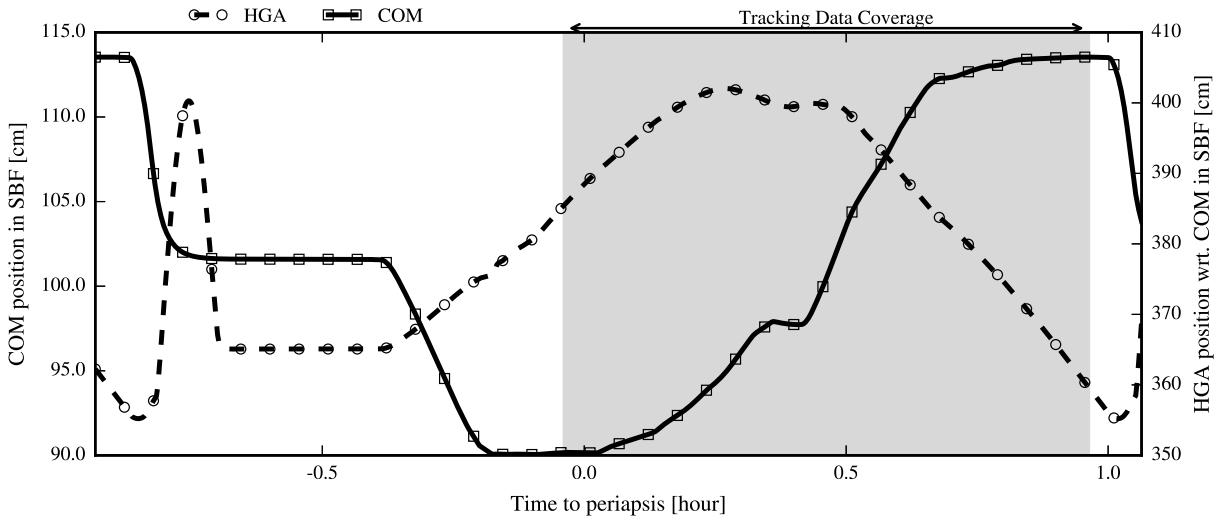

Fig. 4 Center of mass displacement

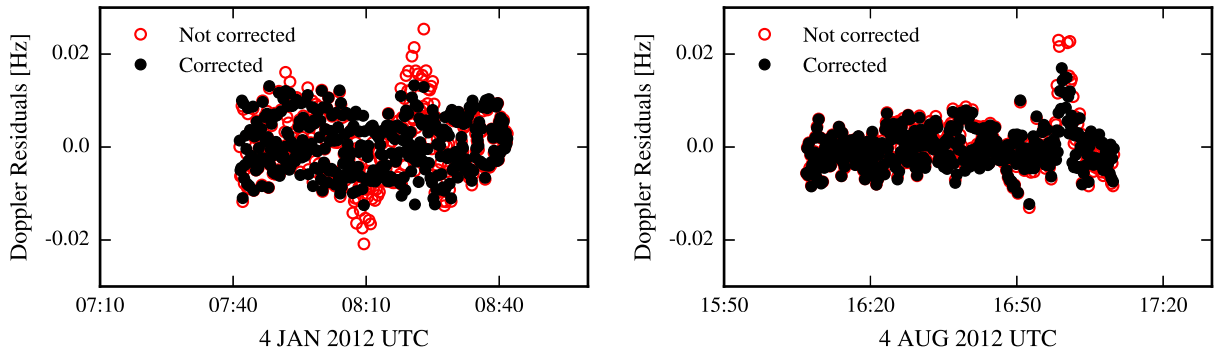

Fig. 5 MRO Doppler Residuals

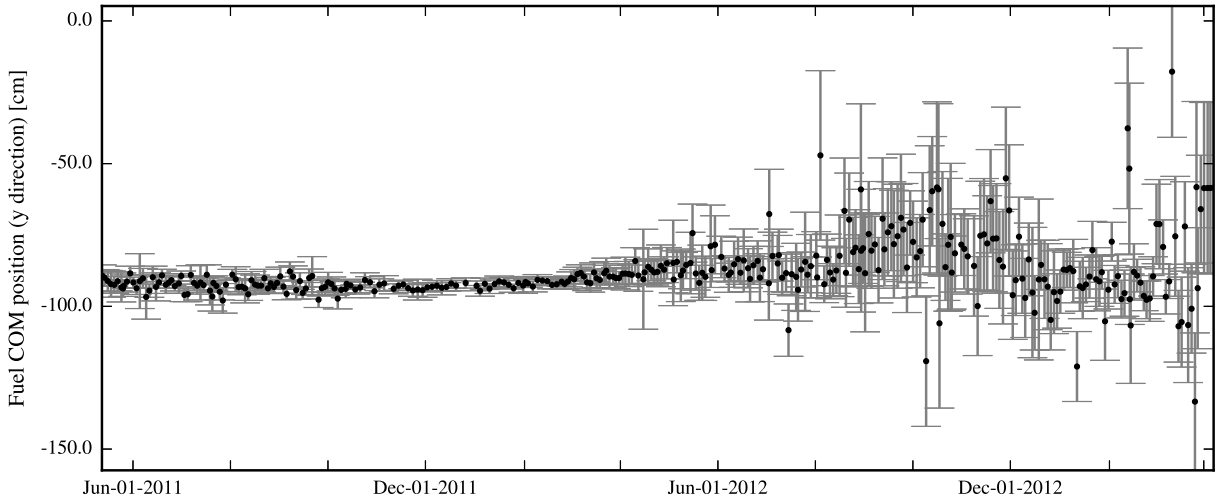

Fig. 6 Fuel CoM estimated position

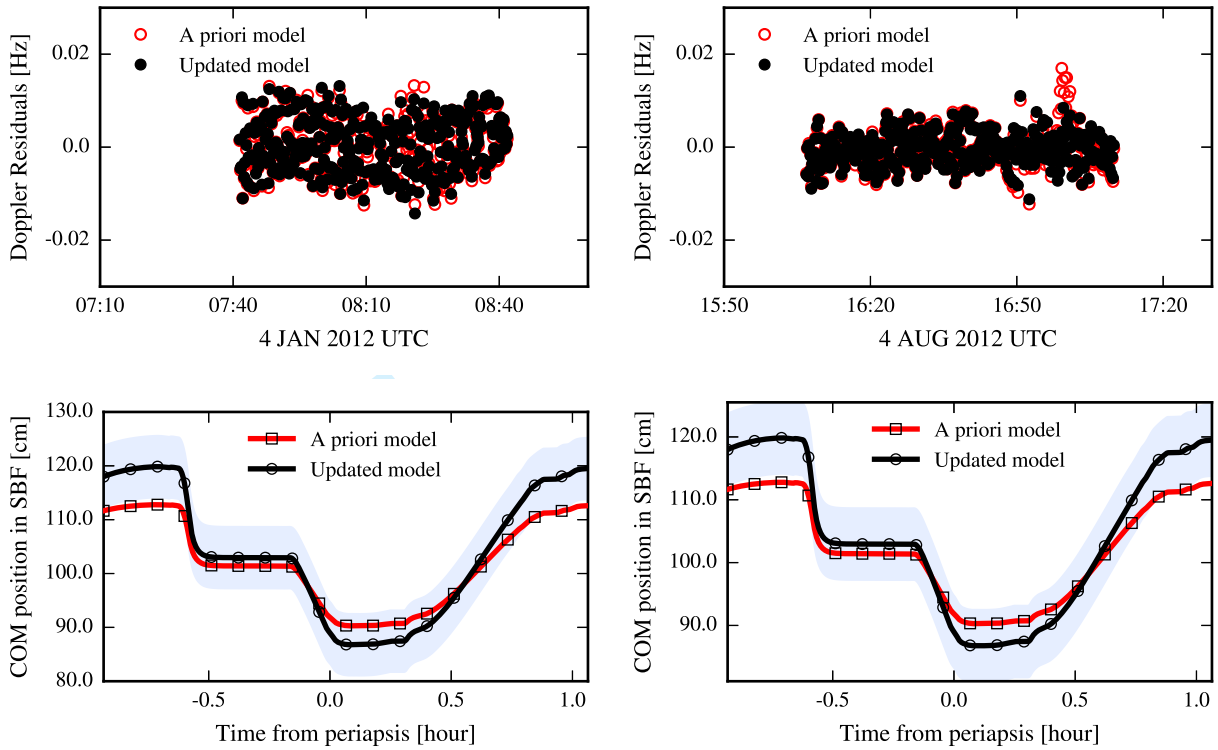

Fig. 7 Doppler residuals and CoM displacement after fit

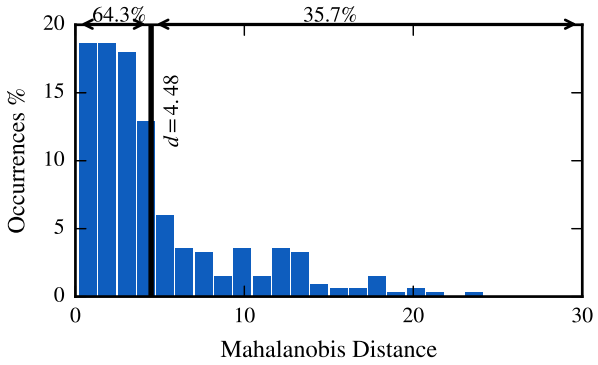

Fig. 8 Spacecraft state vector statistical consistency

Table 1 Filter Setup

Parameter	Group
$\mathbf{r}_{FUEL}$	Local
$\mathbf{r}_{BUS}$	Global
$\mathbf{r}_{HGA}$	
$\mathbf{r}_{HGA_{IG}}$	
$\mathbf{r}_{HGA_{OG}}$	
$\mathbf{r}_{SAPX}$	
$\mathbf{r}_{SAMX}$	
$\mathbf{r}_{HGA_{BP}}$	Consider
$\mathbf{r}_{HELIUM}$	
$\mathbf{r}_{SAPX_{BP}}$	
$\mathbf{r}_{SAMX_{BP}}$	

Table 2 Filter results

Parameter	Delta (m)	Formal Uncertainty (m)
$\mathbf{r}_{SAPX}(X)$	-1.1801	$5.0e-3$
$\mathbf{r}_{SAPX}(Y)$	$6.7e-3$	$3.5e-3$
$\mathbf{r}_{SAPX}(Z)$	$2.9e-5$	$1.5e-4$
$\mathbf{r}_{SAMX}(X)$	-1.2510	$2.6e-3$
$\mathbf{r}_{SAMX}(Y)$	$2.55e-2$	$3.4e-3$
$\mathbf{r}_{SAMX}(Z)$	$5.0e-5$	$1.5e-4$
$\mathbf{r}_{BUS}(X)$	$2.6e-5$	$9.9e-4$
$\mathbf{r}_{BUS}(Y)$	$6.3e-2$	$1.5e-1$
$\mathbf{r}_{BUS}(X)$	$1.5e-2$	$1.1e-2$
$\mathbf{r}_{HGA}(X)$	$1.4e-3$	$8.2e-2$
$\mathbf{r}_{HGA}(Y)$	$-4.3e-1$	$1.1e-2$
$\mathbf{r}_{HGA}(Z)$	$1.3e-2$	$9.9e-2$
$\mathbf{r}_{IG}(X)$	$4.0e-4$	$7.0e-2$
$\mathbf{r}_{IG}(Y)$	$1.38e-2$	$8.40e-2$
$\mathbf{r}_{IG}(Z)$	$4.8e-4$	$7.0e-2$
$\mathbf{r}_{OG}(X)$	$1.4e-3$	$8.2e-2$
$\mathbf{r}_{OG}(Y)$	$1.4e-2$	$8.4e-2$
$\mathbf{r}_{IG}(Z)$	$1.5454e-2$	$6.1e-4$
$\mathbf{r}_{SAMX_{BP}}(X,Y,Z)$	–	$1.0e-1$
$\mathbf{r}_{SAPX_{BP}}(X,Y,Z)$	–	$1.0e-1$
$\mathbf{r}_{HGA_{BP}}(X,Y,Z)$	–	$8.0e-2$
$\mathbf{r}_{HELIUM}(X,Y,Z)$	–	$1.0e-1$

References

[1] Cappuccio, P., Di Ruscio, A., Iess, L., and Mariani, M. J., "BepiColombo Gravity and Rotation Experiment in a Pseudo Drag-Free System," 2020. https://doi.org/10.2514/6.2020-1095.

[2] Imperi, L., Iess, L., and Mariani, M. J., "An analysis of the geodesy and relativity experiments of {BepiColombo}," *Icarus*, Vol. 301, 2018, pp. 9–25. https://doi.org/10.1016/j.icarus.2017.09.008.

[3] Schulte, H., Bell, H., Becker, T., and Best, R., "ISA-MORE Measurement Interface - BC-ASD-TN-00090," Tech. rep., EADS Astrium, 2007.

[4] Lee, A. Y., and Wertz, J. A., "In-Flight Estimation of the Cassini Spacecraft's Inertia Tensor," *Journal of Spacecraft and Rockets*, Vol. 39, No. 1, 2002, pp. 153–155. https://doi.org/10.2514/2.3795.

[5] Thienel, J. K., Luquette, R. J., and Sanner, R. M., "Estimation of spacecraft inertia parameters," *AIAA Guidance, Navigation and Control Conference and Exhibit*, 2008. https://doi.org/10.2514/6.2008-6454.

[6] Biondi, G., Mauro, S., and Pastorelli, S., "Kinematic registration and shape analysis for locating center of mass in large passive spacecraft," *2017 IEEE International Workshop on Metrology for AeroSpace (MetroAeroSpace)*, IEEE, 2017, pp. 50–55. https://doi.org/10.1109/MetroAeroSpace.2017.7999537.

[7] Aghili, F., Kuryllo, M., Okouneva, G., and English, C., "Fault-Tolerant Position/Attitude Estimation of Free-Floating Space Objects Using a Laser Range Sensor," *IEEE Sensors Journal*, Vol. 11, No. 1, 2011, pp. 176–185. https://doi.org/10.1109/JSEN.2010.2056365.

[8] Jun, Z., He, H., and Yingying, L., "Spacecraft center of mass online estimation based on multi-accelerometers," *2010 2nd IEEE International Conference on Information Management and Engineering*, IEEE, 2010, pp. 295–298. https://doi.org/10.1109/ICIME.2010.5478078.

[9] Palimaka, J., and Burlton, B., "Estimation of spacecraft mass properties using angular rate gyro data," *Guidance, Navigation and Control Conference*, American Institute of Aeronautics and Astronautics, Reston, Virigina, 1992. https://doi.org/10.2514/6.1992-4365.

[10] Barbaglio, F., Armstrong, J. W., and Iess, L., "Precise Doppler Measurements for Navigation and Planetary Geodesy Using Low Gain Antennas: Test Results from Cassini," *23rd International Symposium on Space Flight Dynamics (ISSFD), Pasadena (CA)*, 2012.

[11] Sedlak, J. E., "Center of mass estimation for a spinning spacecraft using doppler shift of the GPS carrier frequency," *AIAA/AAS Astrodynamics Specialist Conference, 2016*, 2016. https://doi.org/10.2514/6.2016-5519.

[12] Moyer, T. D., *Formulation for Observed and Computed Values of Deep Space Network Data Types for Navigation*, John Wiley & Sons, Inc., Hoboken, NJ, USA, 2003. https://doi.org/10.1002/0471728470.

[13] Tapley, B. D., Schutz, B. E., and Born, G. H., *Statistical Orbit Determination*, Elsevier, United States, 2004. https://doi.org/10.1016/B978-0-12-683630-1.X5019-X.

[14] Gibbs, B. P., *Advanced Kalman Filtering, Least-Squares and Modeling*, John Wiley & Sons, Inc., Hoboken, NJ, USA, 2011. https://doi.org/10.1002/9780470890042.

[15] Graf, J. E., Zurek, R. W., Eisen, H. J., Jai, B., Johnston, M., and DePaula, R., "The Mars Reconnaissance Orbiter Mission," *Acta Astronautica*, Vol. 57, No. 2-8, 2005, pp. 566–578. https://doi.org/10.1016/j.actaastro.2005.03.043.

[16] Zuber, M. T., Lemoine, F. G., Smith, D. E., Konopliv, A. S., Smrekar, S. E., and Asmar, S. W., "Mars Reconnaissance Orbiter Radio Science Gravity Investigation," *Journal of Geophysical Research*, Vol. 112, No. E5, 2007, p. E05S07. https://doi.org/10.1029/2006JE002833.

[17] Konopliv, A. S., Asmar, S. W., Folkner, W. M., Karatekin, O., Nunes, D. C., Smrekar, S. E., Yoder, C. F., and Zuber, M. T., "Mars high resolution gravity fields from MRO, Mars seasonal gravity, and other dynamical parameters," *Icarus*, Vol. 211, No. 1, 2011, pp. 401–428. https://doi.org/10.1016/j.icarus.2010.10.004.

[18] Genova, A., Goossens, S., Lemoine, F. G., Mazarico, E., Neumann, G. A., Smith, D. E., and Zuber, M. T., "Seasonal and static gravity field of Mars from MGS, Mars Odyssey and MRO radio science," *Icarus*, Vol. 272, 2016, pp. 228–245. https://doi.org/10.1016/j.icarus.2016.02.050.

[19] Konopliv, A. S., Park, R. S., and Folkner, W. M., "An improved JPL Mars gravity field and orientation from Mars orbiter and lander tracking data," *Icarus*, Vol. 274, 2016, pp. 253–260. https://doi.org/10.1016/j.icarus.2016.02.052, URL https://linkinghub.elsevier.com/retrieve/pii/S0019103516001305.

[20] Zurek, R. W., and Smrekar, S. E., "An overview of the Mars Reconnaissance Orbiter (MRO) science mission," *Journal of Geophysical Research*, Vol. 112, No. E5, 2007, p. E05S01. https://doi.org/10.1029/2006JE002701.

[21] Highsmith, D., You, T.-H., Demcak, S., Graat, E., Higa, E., Long, S., Bhat, R., Mottinger, N., Halsell, A., and Peralta, F., "Mars Reconnaissance Orbiter Navigation During the Primary Science Phase," *AIAA/AAS Astrodynamics Specialist Conference and Exhibit*, American Institute of Aeronautics and Astronautics, Reston, Virigina, 2008. https://doi.org/10.2514/6.2008-6422.

[22] Milani, A., and Gronchi, G., *Theory of Orbit Determination*, Cambridge University Press, Cambridge, 2009. https://doi.org/10.1017/CBO9781139175371.

[23] Kass, D. M., Kleinböhl, A., McCleese, D. J., Schofield, J. T., and Smith, M. D., "Interannual similarity in the Martian atmosphere during the dust storm season," *Geophysical Research Letters*, 2016. https://doi.org/10.1002/2016GL068978.

[24] Mazarico, E., Zuber, M. T., Lemoine, F. G., and Smith, D. E., "Effects of self-shadowing on nonconservative force modeling for mars-orbiting spacecraft," *Journal of Spacecraft and Rockets*, 2009. https://doi.org/10.2514/1.41679.

[25] Gallego, G., Cuevas, C., Mohedano, R., and García, N., "On the mahalanobis distance classification criterion for multidimensional normal distributions," *IEEE Transactions on Signal Processing*, 2013. https://doi.org/10.1109/TSP.2013.2269047.